G Suraishkumar ORCID iD: 0000-0002-6521-4494

Mechanism of the oxidative stress mediated increase in lipid accumulation by the bacterium, *R. opacus* PD630: Experimental analysis and genome-scale metabolic modeling

Archanaa Sundararaghavan[1], Amitava Mukherjee[2], Swagatika Sahoo[3]*, G. K. Suraishkumar[1]*

[1]Department of Biotechnology, Bhupat and Jyoti Mehta School of Biosciences building

Indian Institute of Technology Madras, Chennai 600036 India

[2]Centre for Nanobiotechnology, VIT University, Vellore 632014 India

[3]Department of Chemical Engineering and Initiative for Biological Systems Engineering Indian Institute of Technology Madras, Chennai 600036 INDIA

Correspondence

G. K. Suraishkumar, Department of Biotechnology, Bhupat and Jyoti Mehta School of Biosciences building, Indian Institute of Technology Madras, Chennai 600036 India.

E–mail: gk@iitm.ac.in Phone: +91 44 2257 4105 Fax: +91 44 2257 4102

ORCID ID: 0000–0002–6521–4494

Swagatika Sahoo, Department of Chemical Engineering and Initiative for Biological Systems Engineering, Indian Institute of Technology Madras, Chennai 600036 INDIA

E-mail: swagatika05@gmail.com

This article has been accepted for publication and undergone full peer review but has not been through the copyediting, typesetting, pagination and proofreading process, which may lead to differences between this version and the Version of Record. Please cite this article as doi: 10.1002/bit.27330.

Funding information

Department of Science and Technology, Government of India, Grant number: SB/S3/CE/007/2013; Department of Biotechnology, Ministry of Science and Technology, Government of India, DBT, Grant number: BT/PR11328/PBD/26/176/2008

Abstract

Appropriate species of oleaginous bacteria, with their high growth rates and lipid accumulation capabilities, can be good contenders for industrial triacylglycerol (TAG) production, compared to microalgae. Further, oxidative stress (OS) can be used to significantly increase TAG yields in oleaginous microbes, but the mechanism is unexplored. In a first, this study explored the mechanism behind OS-mediated increase in TAG accumulation by the bacterium, *R. opacus* PD630, through experimental analysis and metabolic modelling. Two mechanisms that could increase acetyl-CoA (TAG-precursor) levels were hypothesized based on literature information. One was OS-mediated inactivation of the aconitase (TCA cycle), and another was the inactivation of the triosephosphate isomerase (TPI; glycolysis). The results negated the involvement of aconitase in increased acetyl-CoA levels. Analysis of the metabolic model showed that inactivation of TPI, re-routed the flux through the pentose phosphate pathway (PPP), supplying both NADPH and acetyl-CoA for TAG synthesis. Additionally, inactivation of TPI increased TAG flux by 143%, whereas, inactivating both TPI and aconitase, increased it by 152%. We present experimental evidence for OS–mediated decrease in TPI activity and increase in activity of glucose-6-phosphate dehydrogenase (PPP

enzyme). The findings indicate that increased flux through PPP can be explored to improve TAG accumulation on a large-scale.

Keywords: Oxidative stress, lipid accumulation in *Rhodococcus*, Acetyl-CoA, Genome-scale metabolic modelling, TPI

Introduction

Bacteria are better contenders for industrial triacylglycerol production compared to microalgae (Archanaa, Jose, Mukherjee, & Suraishkumar, 2019). The growth rate of the relevant bacterial species such as *Rhodococcus* is about 25-fold higher than microalgae such as *Chlorella*, and the bacterial productivity is 75-fold higher (Archanaa et al., 2019). The productivities can be significantly improved further through oxidative stress (OS) by reactive species (RS) induction (Balan & Suraishkumar, 2014; Menon, Balan, & Suraishkumar, 2013).

In a biological system, RS such as hydroxyl ($^{\cdot}OH$), superoxide ($O_2^{\cdot-}$) and hydrogen peroxide (H_2O_2) play vital roles in cellular processes through cell signaling and other means (Halliwell & Gutteridge, 2015). They are constantly produced and eliminated in the cell, and if their production rate exceeds their elimination rate to cause their accumulation, the result is OS (Gupta et al., 2012). OS causes cytotoxicity by inducing damage to proteins, lipids, and DNA (Mathur et al., 2015; Shukla et al., 2011). Nevertheless, OS have also been found to be beneficial because their careful induction improves the production of industrially valuable products such as polyhydroxy butyrate (PHB) and biofuel precursor such as triacylglycerol (TAG), a neutral lipid molecule (Al Rowaihi et al., 2018; Balan & Suraishkumar, 2014).

OS-mediated improvement of lipid accumulation in oleaginous microbes such as yeast (Yu et al., 2015) and microalgae have been widely reported (Balan & Suraishkumar, 2014; Menon et al., 2013; Yilancioglu, Cokol, Pastirmaci, Erman, & Cetiner, 2014). The effects of many environmental stress factors such as nutrient limitation, pH or temperature are known to be mediated through OS (Menon et al., 2013; Sarkar & Suraishkumar, 2011) and their role in improved lipid accumulation has been suggested (Liu, Huang, Li, Xia, & Chen, 2012; Xin, Hong-ying, & Yu-ping, 2011). A positive relationship has been established between OS and lipid accumulation in green alga *Chlorella* subjected to low nitrogen stress (Fan, Cui, Wan, Wang, & Li, 2014; Y. M. Zhang, Chen, He, & Wang, 2013). Similarly, with oleaginous bacteria *Rhodococccus opacus* PD630, we observed a concomitant increase in TAG content with an increase in OS (Sundararaghavan, Mukherjee, & Suraishkumar, 2019). Though there is evidence to substantiate the involvement of OS in lipid accumulation, the specific mechanism involved lacks experimental evidence and has been rarely investigated (Shi et al., 2017). The current study is aimed at understanding the role of OS in TAG accumulation by *R. opacus* PD630.

Several studies have reported that the TCA cycle enzyme aconitase (ACO; EC 4.2.1.3) that interconverts citrate to isocitrate is a major target of OS, as the latter inhibits them by oxidizing the iron-sulfur (FeS) cluster present at their catalytic site (Abela et al., 2017; Tong & Rouault, 2007). As a potential target of RS, aconitase activity has also been widely used as an OS marker (Rose et al., 2012). The inactivation of aconitase has been reported to shift metabolism towards lipid synthesis by rerouting the citrate flux towards the lipid precursor molecule, acetyl-CoA (A–CoA) formation (Hurd et al., 2012; Quijano,

Trujillo, Castro, & Trostchansky, 2016). OS-mediated increase in lipid accumulation in rat livers has already been reported (Armstrong, Whiteman, Yang, & Jones, 2004). Nevertheless, inter-correlation between intracellular levels of reactive species, A–CoA and aconitase activity have not been established. Thus, in the current study, a similar mechanism of OS-mediated increase in TAG was hypothesized in *R. opacus* PD630, and above-mentioned correlations were established.

This study is first of its kind to investigate the role of OS in lipid accumulation with a specific interest on the oleaginous bacteria. As OS is a common mediator of lipid accumulation under various stresses such as pH, light, nutrients etc. (Fan et al., 2014; Liu et al., 2012), understanding their mode of action is of significance and can help in identifying potential gene targets for strain improvement (Yilancioglu et al., 2014)

Further, genome-scale metabolic modelling (GSM) of *Rhodococcus* has been carried out to understand the role of OS in TAG accumulation. GSM of various organisms and cell lines have been built and used for many biotechnological purposes (Palsson, 2015; C. Zhang & Hua, 2016; Calmels, McCann, Malphettes, & Andersen, 2019). In this study, GSM analysis of *R. opacus* PD630 predicted an alternative mechanism of OS-mediated increase in TAG accumulation which was then experimentally validated. Specifically, inhibition of the glycolytic enzyme triosephosphate isomerase (TPI; EC 5.3.1.1) and rerouting of metabolism through pentose phosphate pathway (PPP) have been analyzed.

Materials and methods

Organism

Rhodococcus opacus PD630 (Alvarez, Mayer, Fabritius, & Steinbüchel, 1996) procured from DSMZ (#44193; culture collections; Germany) was cultivated in nutrient broth (NB) at 28 ˚C and 200 rpm as detailed in our previous work (Archanaa et al., 2019). Samples taken at the 12th hour, at which time the TAG content was maximum (Archanaa et al., 2019), were analyzed.

Oxidative stress and TAG measurement

Nano-TiO_2 that are known to induce OS in biological systems (Mathur et al., 2015) was used at different concentrations and different Ultraviolet-B (UVB) light conditions (Schematic S1) as previously reported (Sundararaghavan et al., 2019) to generate various levels of OS in *R. opacus* PD630. The OS was measured by quantifying specific intracellular levels of hydroxyl radicals (si–OH), the most reactive among the free radicals (Maurya, 2013). The protocol followed is given in supplementary file 1.

The TAG was converted to fatty acid methyl esters (FAME) through *in situ* transesterification of biomass, as previously reported (Archanaa et al., 2019). The resulting FAME was quantified by gravimetry and expressed in percentage cell dry weight (CDW).

Acetyl-CoA extraction and quantification

The cell pellet equivalent to 5 OD units obtained from 12th hour of cultivation was washed with ice-cold 0.85% NaCl (RM 853, Himedia, Mumbai, India), and snap frozen in liquid nitrogen. Immediately after, they were stored at –80^{o}C, and analyzed later. The A–CoA extraction and quantification have been detailed in supplementary file 1.

Enzyme assays

The kinetic assay of TCA cycle enzyme aconitase was performed based on the protocol of Henson and Cleland (1967) using citric acid. The glycolytic enzyme, TPI, was assayed as per the protocol of Maitra and Lobo (1971). The kinetic assay of pentose phosphate pathway (PPP) enzyme glucose-6-phosphate dehydrogenase (G6PDH; EC 1.1.1.49) was performed with the procedure documented by SIGMA-ALDRICH that had been devised based on the protocol of Noltmann et al., (1961). The assay protocol, reagents used, and the reaction mixture details for all three enzymes are elaborated in supplementary file 1.

GSM model reconstruction

The GSM model of *R. jostii* RHA1 (iMT1174) provided by Tajparast and Frigon (2015), a close relative of *R. opacus* PD630 (Holder et al., 2011) was used in this study. BLAST analysis revealed that the strains had a genome similarity of 96%. The size of the iMT1174 model was 1935 reactions and 1243 metabolites. The iMT1174 was reconstructed to suit *R. opacus* PD630 as described in supplementary file 1. The GSM was analyzed in the MATLAB R2018b (Mathworks Inc., Natick, MA, USA) environment using COBRA toolbox v.3.0 (Heirendt et al., 2019) with Gurobi v.8.1.1 as the linear programming solver. The reconstructed model ‘RO PD 630’ (SBML format) can be found in supplementary file 2.

Model simulations

The simulations performed in the reconstructed model involved Pareto optimization analysis (Oberhardt, Goldberg, Hogardt, & Papin, 2010)and minimization of metabolic adjustments (MOMA) (Segre, Vitkup, & Church, 2002) using in-built functions in the COBRA toolbox. The carbon source (glucose) uptake rate was constrained to 4.5 mmol g^{-1} h^{-1}, based on experimental observation. The objective functions assigned were biomass reaction, TAG storage, and their combination.

Pareto optimum curve construction

In an oleaginous organism, the biomass production and lipid accumulation often conflict with each other. Improvement in any one of them may not be possible without compromising on the other. For instance, improved lipid accumulation in algae was associated with a decrease in biomass (Singh et al., 2016). In the current study, initially flux balance analysis (FBA) that predicts the steady state reaction flux was performed with the model to optimize the objective functions (Orth, Thiele, & Palsson, 2010). The FBA simulation showed that the optimization of either of the objective function happened at the expense of other (Table S1), as the growth and lipid accumulation are not coupled process in general. However, since *R. opacus* PD630 grown in NB showed simultaneous growth and lipid accumulation (Archanaa et al., 2019), a Pareto simulation (Byrne, Dumitriu, & Segrè, 2012; Oberhardt et al., 2010) was performed to analyze them. Pareto optimality analysis would allow us to optimize the two objectives simultaneously and depicts the trade-off between them. The Pareto optimum curve was constructed by fixing the biomass flux at a different level, and the TAG storage flux was optimized at each

level. Pareto plot can also show the possibility for improvement in one objective without trading off with others.

MOMA-Analysis of perturbations

MOMA simulation is performed to analyze the metabolic flux distribution under perturbed conditions such as OS. Under circumstances of change in optimal growth conditions or genetic modifications, the organism would undergo minimal flux redistribution w.r.t to optimal growth flux. The minimization happens to reduce the cellular effort in utilizing the available energy resources and to efficiently make use of the available biochemical reactions (Holzhütter, 2004; Segre et al., 2002). The minimized fluxes of perturbed metabolic network predicted through MOMA's quadratic programming highly correlates with experimental fluxes when compared to the predictions through FBA (Segre et al., 2002). The FBA analysis of 'RO PD 630' model showed optimal growth when there was no TAG accumulation, during which C/N uptake rate ratio was 1.5:1. The TAG storage in the model was facilitated by limiting the nitrogen (ammonium) uptake rate based on the experimental conditions, such that the C/N uptake ratio was 3:1. Thus, to better capture the flux distribution under this condition during which the growth will be suboptimal with simultaneous TAG storage, MOMA was performed w.r.t excess nitrogen condition (1.5:1). Tajparast and Frigon (2015) reported that the storage fluxes under N-limited condition in *R. jostii* were predicted better with MOMA, than FBA. While performing MOMA, maximization of growth was adopted as an objective function for nitrogen excess condition and maximization of both growth and TAG was the objective function for N-limited condition.

The OS was mimicked in the N-limited model by constraining the flux through the oxidative targets such as TCA cycle enzyme aconitase and glycolytic enzyme TPI to zero or by reducing the flux by various levels in the range of 20-80%. The flux distribution was analyzed through MOMA. The flux distribution from MOMA analysis of N-limited model as previously described, with unconstrained aconitase and TPI fluxes would serve as a control. While the Pareto analysis would give the range of optimal fluxes that is possible for objectives such as biomass and TAG, it may not reflect the effect of perturbations in the network. Whereas, MOMA would precisely predict the simultaneous effect of perturbations on the fluxes of both the objectives.

Results and discussion

A-CoA positively correlated with oxidative stress

The effect of OS on lipid accumulation has been well recorded (Menon et al., 2013; Yilancioglu et al., 2014; Y. M. Zhang et al., 2013). To understand how OS improves the cellular lipid content, a relation between intracellular levels of lipid precursor molecule A-CoA at various oxidative stress levels (si-OH) was established. As hypothesized, a concomitant increase in A-CoA levels with an increase in si-OH levels was observed (Figure 1a), and with increasing A-CoA a simultaneous increase in FAME content was observed (Figure 1b). Though a few of the values of FAME content remained constant with change in A-CoA levels, the overall trend was positive. The trend shows that OS acted by surging the availability of A-CoA for lipid accumulation. While a positive relationship between A-CoA and lipid accumulation have been widely reported in microalgae (Avidan, Brandis, Rogachev, & Pick, 2015; Huang et al., 2015; Jose &

Suraishkumar, 2016), this study reports it for the first time in oleaginous bacteria such as *Rhodococcus*. Further, the positive correlation between A-CoA and OS reported in the current work have not been explored in any oleaginous species.

Aconitase correlated negatively with oxidative stress but poorly with A-CoA

To further understand how OS would increase the A-CoA levels, the activity of aconitase, which is one of the major stress targets, was measured at different OS levels. As hypothesized, with an increase in OS, the aconitase activity was found to decrease, suggesting OS-mediated inhibition of aconitase (Figure 2a). Likewise, with a decrease in aconitase activity increase in the FAME content was observed (Figure 2b). It has been reported that aconitase inhibition would result in citrate accumulation, which is eventually catalyzed by citrate lyase (CL) (Hurd et al., 2012). The CL converts citrate to A-CoA and plays an important role in lipid synthesis (Aoshima, Ishii, & Igarashi, 2004; Hurd et al., 2012; Quijano et al., 2016). While CL activity is a mammalian and eukaryotic feature, its occurrence is also reported in prokaryotes such as *Hydrogenobacter thermophilus* (Aoshima et al., 2004) and *Rhodococcus* (Alvarez, 2010) performing reductive TCA cycle. Thus, aconitase inhibition due to OS was suspected as a reason behind increased A-CoA in *R. opacus* PD630. The positively correlated A-CoA levels and negatively correlated aconitase activity w.r.t OS seemed to support the same. However, A-CoA levels did not correlate well with aconitase activity and had a greater number of outliers (Figure 3). The poor correlation suggested that OS-mediated aconitase inhibition alone might not have resulted in increased A-CoA levels. It is probably for the same reason that there were few outliers observed in case of aconitase vs. FAME

correlation (Figure 2b). Thus, to better understand the reason for OS-mediated increase in lipid accumulation, a GSM modelling approach was carried out.

Pareto plot: TAG improvement with no compromise on growth

Before analyzing the model for the effect of OS, Pareto analysis was carried out to understand the inter-relationship between simultaneous growth and TAG accumulation of *R. opacus* PD630. The experimentally observed growth rate of *R. opacus* PD630 was in the range of 0.2 h^{-1} (Sundararaghavan et al., 2019). From the Pareto chart, it can be observed that TAG storage flux range (i.e., 0.001 to 0.17 mmol · $(g\ cell)^{-1}$. h^{-1}) is possible without compromising on the growth rate value (i.e., 0.2 h^{-1}), Figure 4. Based on the TAG accumulation period of 12 h, and from the molecular weight of TAG (Triolein) which was around 0.9 g $mmol^{-1}$ (Badu & Awudza, 2017), the TAG storage flux were translated in to TAG content which ranged from 0.01 – 1.9 g · $(g\ cell)^{-1}$ (10% - 190% CDW). From the above range, the practically possible range would include 0.01 – 0.87 g · $(g\ cell)^{-1}$, as *R. opacus* PD630 is capable of accumulating TAG up to a maximum of 87% of its CDW (Holder et al., 2011). Thus, the Pareto analysis revealed the possibility of TAG improvement without trading off with biomass growth. The analysis supports our previous observation wherein the growth remained unaffected at around 0.2 h^{-1}, while the TAG improved from 0.3 to 0.54 g · $(g\ cell)^{-1}$ (30 – 54% CDW) under OS (Sundararaghavan et al., 2019).

Aconitase inactivation does not result in improved TAG

The MOMA analysis showed that the predicted growth rate and TAG storage flux of the control was around 0.2 h^{-1} and 0.022 mmol · $(g\ cell)^{-1}$· h^{-1}, respectively. The predicted

growth rate was strikingly the same as that of experimentally observed growth rate. As already quoted, MOMA predicts fluxes close to experimental fluxes (Segre et al., 2002). The predicted TAG storage flux of the control, when converted to TAG content, was equivalent to 0.24 g · (g cell)$^{-1}$, while the experimentally observed TAG content was around 0.3 g · (g cell)$^{-1}$. Though the two values are not very similar, they are not highly deviated.

When flux through aconitase was constrained to zero ($\overline{ACO}$) to mimic the OS targeted inactivation of aconitase, the growth rate remained unaffected, but no increase in TAG storage flux was observed. The $\overline{ACO}$ had similar TAG storage flux as that of control (Figure 5a). The $\overline{ACO}$ did result in increased flux through citrate lyase (CL: EC 4.1.3.6) that converts citrate to acetate when compared to control (Figure 6f). The eventual conversion of acetate to A-CoA happened through acetate kinase-phosphotransacetylase (AK-PTA) pathway. In the AK-PTA pathway, acetate is converted to acetyl phosphate (ace-P) by acetate kinase (AK; EC 2.7.2.1), which is later converted to A-CoA by phosphotransacetylase (PTA; EC 2.3.1.8) enzyme (Alvarez, 2010). Though $\overline{ACO}$ had higher CL flux when compared to control, the AK-PTA flux was only marginally higher than the control (Figure 6e & 6h) and probably resulted in similar TAG flux. This also explains the poor correlation that was observed between aconitase and A-CoA (Figure 3). From the experiment result and with support from model predictions it can be concluded that though the aconitase activity does decrease under OS, it is not likely to be responsible for increased TAG content in *R. opacus* PD630.

TPI inactivation: a cause for improved TAG

OS is known to inhibit the glycolytic enzyme TPI (Grant, 2008; Ralser et al., 2007), which is linked to PPP pathway via its substrate glyceraldehyde-3-phosphate (g3p) (Trujillo et al., 2014). Inhibition of TPI due to OS reroutes the flux from glycolysis to PPP (Grant, 2008; Ralser et al., 2007). Under OS, rerouting of flux from glycolysis to PPP have been reported to occur in human skin cells (Kuehne et al., 2015). The PPP is an important source for cellular reducing power, i.e., NADPH. The NADPH provides redox power for the most antioxidant system that includes, glutathione/glutaredoxin and thioredoxin systems. Thus, rerouting of flux to PPP to elevate the NADPH levels, occurs as a defense measure against OS (Grant, 2008; Kuehne et al., 2015; Ralser et al., 2007). The first step of the PPP reaction catalyzed by glucose-6-phosphate dehydrogenase is also the major supplier of NADPH for lipid synthesis. As highly reduced molecules, lipid requires an increased amount of NADPH for their overproduction (Wasylenko, Ahn, & Stephanopoulos, 2015). Thus, rerouting of flux through the PPP pathway has been speculated as a possible mechanism of OS dependent increase in lipid accumulation, but lacks evidence (Shi et al., 2017).

In our model, OS mediated inactivation of TPI was mimicked by blocking the flux through TPI (TPI $^{-}$). As hypothesized, shutting off TPI resulted in rerouting of flux through PPP, because TPI $^{-}$ had a G6PDH flux of 1.26 mmol $\cdot$ (g cell)$^{-1}\cdot$ h^{-1}, while the control (with active TPI) had zero G6PDH flux (Figure 6c). The rerouting of flux through G6PDH is believed to have generated the NADPH required for the lipid synthesis. But, for increased lipid synthesis, apart from the cofactor NADPH, continuous supply of their precursor molecule A-CoA is also essential (Yang et al., 2013). However, in the case of

TPI$^-$ the lower glycolytic fluxes and hence the flux through pyruvate dehydrogenase (PDH) that produces A-CoA decreased by around 2-fold and 1.5-fold, respectively (Figure S1). Nevertheless, during flux rerouting from glycolysis to PPP, A-CoA is also expected to be sourced through, xylulose-5-phosphate (x5p), one of the metabolic intermediates of PPP. The x5p is broken down into g3p and ace-P, by phosphoketolase (PK; EC 4.1.2.9) enzyme (de Jong, Shi, Siewers, & Nielsen, 2014). The ace-P is then converted to A-CoA, through AK-PTA pathway, as mentioned in the previous section (Alvarez, 2010).

Further, the upregulation of PK in *Saccharomyces cerevisiae* resulted in enhanced fatty acid production through improved A-CoA provision (de Jong et al., 2014). The production of A-CoA via PK would minimize the carbon and energy loss when compared to the native route of A-CoA production through pyruvate dehydrogenase or pyruvate decarboxylase (Bergman, Siewers, Nielsen, & Chen, 2016). Thus, PK is considered as a thermodynamically efficient and potential candidate for improving the cellular A-CoA levels (Bergman et al., 2016). As seen from figure 6d, in TPI$^-$, the flux through PK was active (1.24 mmol $\cdot$ (g cell)$^{-1}\cdot$ h^{-1}), while in case of control and ACO$^-$ it was zero. The ace-P resulting from PK was then converted to A-CoA via both PTA and acetyl CoA synthetase (ACS; EC 6.2.1.1), whose fluxes were also high when compared to control and ACO$^-$ (Figure 6e and 6g). While for TPI$^-$, the A-CoA production flux via PDH decreased by 1.5-fold as mentioned previously, the A-CoA production flux via PTA increased by 4.3-fold when compared to control (Figure S1), suggesting that increased A-CoA levels could be majorly via PK-PTA actions.

Further, the flux through acetyl-CoA carboxylase carboxyl transferase (ACC; EC 6.4.1.2) that converts A-CoA to malonyl-CoA, were also high in case of TPI^- when compared to control and ACO^- (Figure 6i). Thus, the TAG storage flux of TPI^- improved significantly to 0.053 mmol · $(g\ cell)^{-1}$· h^{-1} which was 143% higher than the control (Figure 5a). As seen from figure 5b, as the flux constrain through TPI increases, a concomitant increase in G6PDH flux and hence, the TAG flux occurs.

Though the ACC flux of ACO^- is also high when compared to control, there is no increase in TAG flux, as there is no active PPP (G6PDH) flux (Figure 6c). This shows that rerouting of flux through PPP pathway can play a significant role in improving the TAG content, as it could supply both NADPH and A-CoA that are necessary for lipid synthesis. While, the model predicted a 143% increase in TAG storage flux when TPI flux is blocked completely, the experimentally observed maximum increase in TAG as reported in our previous study was around 81% (Sundararaghavan et al., 2019). The experimentally observed value suggested partial inhibition of TPI by $nTiO_2$-induced OS.

Aconitase and TPI inactivation synergistically improve TAG

Since OS are known to inhibit both aconitase and TPI, flux through these reactions were blocked (ACO^-TPI^-) to identify their combined effect on TAG storage flux if any. As seen from figure 6c, the flux through G6PDH improved further in case of ACO^-TPI^- when compared to TPI^-. However, the PK and PTA fluxes of ACO^-TPI^- were less when compared to TPI^-. Nevertheless, while both ACO^- and TPI^- had increased ACC flux, their combined inactivation further improved the ACC flux. Thus, TAG storage flux of ACO^-TPI^- improved slightly further by 10% than TPI^- and was 152% higher than the control

(Figure 5a), suggesting synergistic action of inactivated TPI and aconitase. The activation of ACC flux by inactivation of either aconitase or TPI or both have not been reported, which is a novel and significant finding from the current study.

Decreased TPI and increased G6PDH activity under OS

The OS-mediated inhibition of TPI and increased activity of G6PDH were experimentally observed in the sample T_MUV_1000 (Schematic S1), which showed the maximum increase (81%) in TAG content (Sundararaghavan et al., 2019). As observed from Figure 7a, the TPI activity of T_MUV_1000 decreased at 60% of the time points (3 out of 5), when compared to control. The TPI activity decreased by 16%, 10% and 20% at 3rd hour, 9th hour and 11th hour, respectively, as the respective oxidative stress increased by 23%, 38%, and 52% (Table S2), when compared to the control.

Previous studies (Grant, 2008; Ralser et al., 2007) and model analysis from this study showed that TPI inhibition increases the flux through PPP pathway. To understand the same, the activity of the first enzyme of PPP, namely G6PDH, was measured because the defense response to OS-mediated inactivation of TPI is significantly dependent on G6PDH (Grüning, Du, Keller, Luisi, & Ralser, 2014). The G6PDH activity of OS-induced sample was observed to increase at 60% of the time points, when compared to control (Figure 7b). The G6PDH activity increased by 9%, 34% and 33% at 3rd hour, 6th hour and 12th hour, respectively, as the respective oxidative stress increased by 23%, 51%, and 114% (Table S2) when compared to control.

As shown through the model analysis discussed in the previous section, the increased G6PDH flux, followed by increased flux through PK-AK-PTA routes, could be one of

the mechanisms by which OS improved the TAG content in *R. opacus* PD 630. However, only moderate changes were experimentally observed in the TPI and G6PDH activities, and further studies on other possible OS targets and metabolite analysis are needed to gain conclusive insights.

Conclusions

This study proposes a mechanism for OS-mediated increase in TAG accumulation with *R. opacus* PD630 as model oleaginous organism. The predictions from the model and experimental evidence suggest that OS could have improved the TAG content of bacteria by inhibiting TPI and eventual flux reroutes through PPP. Though aconitase inhibition was observed, it did not contribute to improved TAG storage. Interestingly, the model suggests a synergistic role of inhibited aconitase and TPI in TAG improvement. Neither the aconitase nor the TPI inhibition affected bacterial growth. The model-predicted growth rate and TAG content correlated well with experimental results. Further, the study reports a novel finding that flux through ACC which carry over the A-CoA for lipid synthesis, is increased when either of the TPI or aconitase flux or both is inactivated. The outcome of this study suggests that PPP and AK-PTA pathways as potential targets for genetically improving the lipid production in oleaginous bacteria such as *R. opacus* PD630.

Acknowledgments

The authors thank the Department of Science and Technology (DST) and Department of Biotechnology (DBT), Ministry of Science and Technology, Government of India, for

financial assistance. Archanaa Sundararaghavan is thankful to the Ministry of human resource and development (MHRD), Government of India, for the award of the fellowship.

References

Abela, L., Spiegel, R., Crowther, L. M., Klein, A., Steindl, K., Papuc, S. M., … Simmons, T. L. (2017). Plasma metabolomics reveals a diagnostic metabolic fingerprint for mitochondrial aconitase (ACO2) deficiency. *PLoS ONE*, *12*, 1–15. https://doi.org/10.1371/journal.pone.0176363

Al Rowaihi, I. S., Paillier, A., Rasul, S., Karan, R., Grotzinger, S. W., Takanabe, K., & Jorg, E. (2018). Poly (3-hydroxybutyrate) production in an integrated electromicrobial setup: Investigation under stress-inducing conditions. *PLoS ONE*, *13*, e0196079. https://doi.org/10.1371/journal.pone.0196079

Alvarez, H. M. (2010). Central Metabolism of Species of the Genus *Rhodococcus*. In H. M. Alvarez (Ed.), *Biology of Rhodococcus* (pp. 91–108). Springer, Berlin, Heidelberg. https://doi.org/10.1007/978-3-642-12937-7

Alvarez, H. M., Mayer, F., Fabritius, D., & Steinbüchel, A. (1996). Formation of intracytoplasmic lipid inclusions by *Rhodococcus opacus* strain PD630. *Archives of Microbiology*, *165*, 377–386. https://doi.org/10.1007/s002030050341

Alvarez, H. M., Roxana, A. S., Herrero, M., Hernández, M. A., & Villalba, M. S. (2013). Metabolism of triacylglycerols in *Rhodococcus* species: insights from physiology and molecular genetics. *Journal of Molecular Biochemistry*, *2*, 69–78.

Aoshima, M., Ishii, M., & Igarashi, Y. (2004). A novel enzyme, citryl-CoA lyase, catalysing the second step of the citrate cleavage reaction in *Hydrogenobacter thermophilus* TK-6. *Molecular Microbiology*, *52*, 763–770. https://doi.org/10.1111/j.1365-2958.2004.04010.x

Archanaa, S., Jose, S., Mukherjee, A., & Suraishkumar, G. K. (2019). Sustainable Diesel Feedstock: a Comparison of Oleaginous Bacterial and Microalgal Model Systems. *Bioenergy Research*, *12*, 205–216. https://doi.org/10.1007/s12155-018-9948-6

Armstrong, J. S., Whiteman, M., Yang, H., & Jones, D. P. (2004). The redox regulation of intermediary metabolism by a superoxide-aconitase rheostat. *BioEssays*, *26*, 894–900. https://doi.org/10.1002/bies.20071

Avidan, O., Brandis, A., Rogachev, I., & Pick, U. (2015). Enhanced acetyl-CoA production is associated with increased triglyceride accumulation in the green alga *Chlorella desiccata*. *Journal of Experimental Botany*, *66*, 3725–3735. https://doi.org/10.1093/jxb/erv166

Badu, M., & Awudza, A. M. J. (2017). Determination of the triacylglycerol content for the identification and assessment of purity of shea butter fat, peanut oil, and palm kernel oil using maldi-tof/tof mass spectroscopic technique. *International Journal of Food Properties*, *20*, 271–280. https://doi.org/10.1080/10942912.2016.1155056

Balan, R., & Suraishkumar, G. K. (2014). Simultaneous increases in specific growth rate and specific lipid content of *Chlorella vulgaris* through UV-induced reactive species. *Biotechnology Progress*, *30*, 291–299. https://doi.org/10.1002/btpr.1854

Bergman, A., Siewers, V., Nielsen, J., & Chen, Y. (2016). Functional expression and evaluation of heterologous phosphoketolases in *Saccharomyces cerevisiae*. *AMB Express*, *6*, 115. https://doi.org/10.1186/s13568-016-0290-0

Byrne, D., Dumitriu, A., & Segrè, D. (2012). Comparative multi-goal tradeoffs in systems engineering of microbial metabolism. *BMC Systems Biology*, *6*, 127. https://doi.org/10.1186/1752-0509-6-127

Calmels, C., McCann, A., Malphettes, L., & Andersen, M. R. (2019). Application of a curated genome-scale metabolic model of CHO DG44 to an industrial fed-batch process. *Metabolic Engineering*, *51*, 9–19. https://doi.org/10.1016/j.ymben.2018.09.009

de Jong, B. W., Shi, S., Siewers, V., & Nielsen, J. (2014). Improved production of fatty acid ethyl esters in *Saccharomyces cerevisiae* through up-regulation of the ethanol degradation pathway and expression of the heterologous phosphoketolase pathway. *Microbial Cell Factories*, *13*, 39. https://doi.org/10.1186/1475-2859-13-39

Fan, J., Cui, Y., Wan, M., Wang, W., & Li, Y. (2014). Lipid accumulation and biosynthesis genes response of the oleaginous *Chlorella pyrenoidosa* under three nutrition stressors. *Biotechnology for Biofuels*, *7*, 17. https://doi.org/10.1186/1754-6834-7-17

Grant, C. M. (2008). Metabolic reconfiguration is a regulated response to oxidative stress. *Journal of Biology*, *7*, 6–9. https://doi.org/10.1186/jbiol63

Grüning, N. M., Du, D., Keller, M. A., Luisi, B. F., & Ralser, M. (2014). Inhibition of

triosephosphate isomerase by phosphoenolpyruvate in the feedback-regulation of glycolysis. *Open Biology*, 4, 130232. https://doi.org/10.1098/rsob.130232

Gupta, S. C., Hevia, D., Patchva, S., Park, B., Koh, W., & Aggarwal, B. B. (2012). Upsides and Downsides of Reactive Oxygen Species for Cancer: The Roles of Reactive Oxygen Species in Tumorigenesis, Prevention, and Therapy. *Antioxidants & Redox Signaling*, *16*, 1295–1322. https://doi.org/10.1089/ars.2011.4414

Halliwell, B., & Gutteridge, J. M. (2015). *Free radicals in biology and medicine By Barry Halliwell and John M. C. Gutteridge.* (5th ed.). Oxford Univeristy Press, New York.

Heirendt, L., Arreckx, S., Pfau, T., Mendoza, S. N., Richelle, A., Heinken, A., … Fleming, R. M. T. (2019). Creation and analysis of biochemical constraint-based models using the COBRA Toolbox v.3.0. *Nature Protocols*, *14*, 639–702. https://doi.org/10.1038/s41596-018-0098-2

Henson, C. P., & Cleland, W. (1967). Purification and Kinetic Studies of Beef Liver Cytoplasmic Aconitase. *Liver*, *242*, 3833–3838.

Hernández, M. A., Mohn, W. W., Martínez, E., Rost, E., Alvarez, A. F., & Alvarez, H. M. (2008). Biosynthesis of storage compounds by *Rhodococcus jostii* RHA1 and global identification of genes involved in their metabolism. *BMC Genomics*, *9*, 600. https://doi.org/10.1186/1471-2164-9-600

Holder, J. W., Ulrich, J. C., Debono, A. C., Godfrey, P. A., Desjardins, C. A., Zucker, J., … Sinskey, A. J. (2011). Comparative and Functional Genomics of *Rhodococcus*

opacus PD630 for Biofuels Development. *PLoS Genetics*, *7*, e1002219. https://doi.org/10.1371/journal.pgen.1002219

Holzhütter, H. G. (2004). The principle of flux minimization and its application to estimate stationary fluxes in metabolic networks. *European Journal of Biochemistry*, *271*, 2905–2922. https://doi.org/10.1111/j.1432-1033.2004.04213.x

Huang, Y., Cheng, J., Lu, H., Huang, R., Zhou, J., & Cen, K. (2015). Simultaneous enhancement of microalgae biomass growth and lipid accumulation under continuous aeration with 15% CO_2. *RSC Advances*, *5*, 50851–50858. https://doi.org/10.1039/c5ra08401f

Hurd, T. R., Collins, Y., Abakumova, I., Chouchani, E. T., Baranowski, B., Fearnley, I. M., … James, A. M. (2012). Inactivation of Pyruvate Dehydrogenase Kinase 2 by Mitochondrial Reactive Oxygen Species. *Journal of Biological Chemistry*, *287*, 35153–35160. https://doi.org/10.1074/jbc.m112.400002

Jose, S., & Suraishkumar, G. K. (2016). High carbon (CO_2) supply leads to elevated intracellular acetyl CoA levels and increased lipid accumulation in *Chlorella vulgaris*. *Algal Research*, *19*, 307–315. https://doi.org/10.1016/j.algal.2016.08.011

Kuehne, A., Emmert, H., Soehle, J., Winnefeld, M., Fischer, F., Wenck, H., … Zamboni, N. (2015). Acute Activation of Oxidative Pentose Phosphate Pathway as First-Line Response to Oxidative Stress in Human Skin Cells. *Molecular Cell*, *59*, 359–371. https://doi.org/10.1016/j.molcel.2015.06.017

Liu, W., Huang, Z., Li, P., Xia, J., & Chen, B. (2012). Formation of triacylglycerol in

Nitzschia closterium f. minutissima under nitrogen limitation and possible physiological and biochemical mechanisms. *Journal of Experimental Marine Biology and Ecology*, *418–419*, 24–29. https://doi.org/10.1016/j.jembe.2012.03.005

Maitra, P., & Lobo, Z. (1971). A Kinetic Study of Glycolytic Synthesis in Yeast. *Biological Chemistry*, *246*, 475–488.

Mathur, A., Raghavan, A., Chaudhury, P., Johnson, J. B., Roy, R., Kumari, J., … Mukherjee, A. (2015). Cytotoxicity of titania nanoparticles towards waste water isolate *Exiguobacterium acetylicum* under UVA, visible light and dark conditions. *Journal of Environmental Chemical Engineering*, *3*, 1837–1846. https://doi.org/10.1016/j.jece.2015.06.026

Maurya, P. K. (2013). Animal Biotechnology as a Tool to Understand and Fight Aging. In A. S. Verma & A. Singh (Eds.), *Animal biotechnology: models in discovery and translation* (pp. 177–191). Elsevier Inc, USA. https://doi.org/10.1016/B978-0-12-416002-6.00010-9

Menon, K. R., Balan, R., & Suraishkumar, G. K. (2013). Stress induced lipid production in *Chlorella vulgaris*: Relationship with specific intracellular reactive species levels. *Biotechnology and Bioengineering*, *110*, 1627–1636. https://doi.org/10.1002/bit.24835

Noltmann, E. A., Gubler, C. J., & Kuby, S. A. (1961). Glucose 6-Phosphate Dehydrogenase I. *The Journal of Biological Chemistry*, *236*, 1225–1230.

Oberhardt, M. A., Goldberg, J. B., Hogardt, M., & Papin, J. A. (2010). Metabolic

network analysis of *Pseudomonas aeruginosa* during chronic cystic fibrosis lung infection. *Journal of Bacteriology*, *192*, 5534–5548. https://doi.org/10.1128/JB.00900-10

Orth, J. D., Thiele, I., & Palsson, B. O. (2010). What is flux balance analysis? *Nature Biotechnology*, *28*, 245–248. https://doi.org/10.1038/nbt.1614

Palsson, B. O. (2015). *Systems biology: Constraint-based reconstruction and analysis* (2nd ed.). Cambridge University Press. https://doi.org/10.1017/CBO9781139854610

Quijano, C., Trujillo, M., Castro, L., & Trostchansky, A. (2016). Interplay between oxidant species and energy metabolism. *Redox Biology*, *8*, 28–42. https://doi.org/10.1016/j.redox.2015.11.010

Ralser, M., Wamelink, M. M., Kowald, A., Gerisch, B., Heeren, G., Struys, E. A., … Krobitsch, S. (2007). Dynamic rerouting of the carbohydrate flux is key to counteracting oxidative stress. *Journal of Biology*, *6*, 10. https://doi.org/10.1186/jbiol61

Rose, S., Melnyk, S., Pavliv, O., Bai, S., Nick, T. G., Frye, R. E., & James, S. J. (2012). Evidence of oxidative damage and inflammation associated with low glutathione redox status in the autism brain. *Translational Psychiatry*, *2*, e134-8. https://doi.org/10.1038/tp.2012.61

Sarkar, P., & Suraishkumar, G. K. (2011). pH and temperature stresses in bioreactor cultures: Intracellular superoxide levels. *Industrial and Engineering Chemistry Research*, *50*, 13129–13136. https://doi.org/10.1021/ie200081k

Segre, D., Vitkup, D., & Church, G. M. (2002). Analysis of optimality in natural and perturbed metabolic networks. *Proceedings of the National Academy of Sciences*, *99*, 15112–15117. https://doi.org/10.1073/pnas.232349399

Shi, K., Gao, Z., Shi, T. Q., Song, P., Ren, L. J., Huang, H., & Ji, X. J. (2017). Reactive oxygen species-mediated cellular stress response and lipid accumulation in oleaginous microorganisms: The state of the art and future perspectives. *Frontiers in Microbiology*, *8*, 793. https://doi.org/10.3389/fmicb.2017.00793

Shukla, R. K., Sharma, V., Pandey, A. K., Singh, S., Sultana, S., & Dhawan, A. (2011). ROS-mediated genotoxicity induced by titanium dioxide nanoparticles in human epidermal cells. *Toxicology in Vitro*, *25*, 231–241. https://doi.org/10.1016/j.tiv.2010.11.008

Singh, P., Kumari, S., Guldhe, A., Misra, R., Rawat, I., & Bux, F. (2016). Trends and novel strategies for enhancing lipid accumulation and quality in microalgae. *Renewable and Sustainable Energy Reviews*, *55*, 1–16. https://doi.org/10.1016/j.rser.2015.11.001

Sundararaghavan, A., Mukherjee, A., & Suraishkumar, G. K. (2019). Investigating the potential use of an oleaginous bacterium, *Rhodococcus opacus* PD630, for nano-TiO_2 remediation. *Environmental Science and Pollution Research*. https://doi.org/10.1007/s11356-019-06388-0

Tajparast, M., & Frigon, D. (2015). Genome-scale metabolic model of *Rhodococcus jostii* RHA1 (iMT1174) to study the accumulation of storage compounds during

nitrogen-limited condition. *BMC Systems Biology*, *9*, 43. https://doi.org/10.1186/s12918-015-0190-y

Thomson, N., Summers, D., & Sivaniah, E. (2010). Synthesis, properties and uses of bacterial storage lipid granules as naturally occurring nanoparticles. *Soft Matter*, *6*, 4045–4057. https://doi.org/10.1039/b927559b

Tong, W. H., & Rouault, T. A. (2007). Metabolic regulation of citrate and iron by aconitases: Role of iron-sulfur cluster biogenesis. *BioMetals*, *20*, 549–564. https://doi.org/10.1007/s10534-006-9047-6

Trujillo, C., Blumenthal, A., Marrero, J., Rhee, K. Y., Schnappinger, D., & Ehrt, S. (2014). Triosephosphate isomerase is dispensable *in vitro* yet essential for *Mycobacterium tuberculosis* to establish infection. *MBio*, *5*, e00085-14. https://doi.org/10.1128/mbio.00085-14

Wasylenko, T. M., Ahn, W. S., & Stephanopoulos, G. (2015). The oxidative pentose phosphate pathway is the primary source of NADPH for lipid overproduction from glucose in *Yarrowia lipolytica*. *Metabolic Engineering*, *30*, 27–39. https://doi.org/10.1016/j.ymben.2015.02.007

Xin, L., Hong-ying, H., & Yu-ping, Z. (2011). Growth and lipid accumulation properties of a freshwater microalga *Scenedesmus* sp. under different cultivation temperature. *Bioresource Technology*, *102*, 3098–3102. https://doi.org/10.1016/j.biortech.2010.10.055

Yang, Z. K., Niu, Y. F., Ma, Y. H., Xue, J., Zhang, M. H., Yang, W. D., … Li, H. Y.

(2013). Molecular and cellular mechanisms of neutral lipid accumulation in diatom following nitrogen deprivation. *Biotechnology for Biofuels*, *6*, 67. https://doi.org/10.1186/1754-6834-6-67

Yilancioglu, K., Cokol, M., Pastirmaci, I., Erman, B., & Cetiner, S. (2014). Oxidative stress is a mediator for increased lipid accumulation in a newly isolated *Dunaliella salina* strain. *PLoS ONE*, *9*, e91957. https://doi.org/10.1371/journal.pone.0091957

Yu, Q., Liu, Z., Xu, H., Zhang, B., Zhang, M., & Li, M. (2015). TiO_2 nanoparticles promote the production of unsaturated fatty acids (UFAs) fighting against oxidative stress in *Pichia pastoris*. *RSC Advances*, *5*, 41033–41040. https://doi.org/10.1039/C5RA02366A

Zhang, C., & Hua, Q. (2016). Applications of genome-scale metabolic models in biotechnology and systems medicine. *Frontiers in Physiology*, *6*, 1–8. https://doi.org/10.3389/fphys.2015.00413

Zhang, Y. M., Chen, H., He, C. L., & Wang, Q. (2013). Nitrogen starvation induced oxidative stress in an oil-producing green alga *Chlorella sorokiniana* C3. *PLoS ONE*, *8*, e69225. https://doi.org/10.1371/journal.pone.0069225

Figure legends

Figure 1: Relationship of A-CoA with OS (a) and TAG (FAME) content (b). The intracellular A-CoA levels correlated positively with si-OH and FAME content.

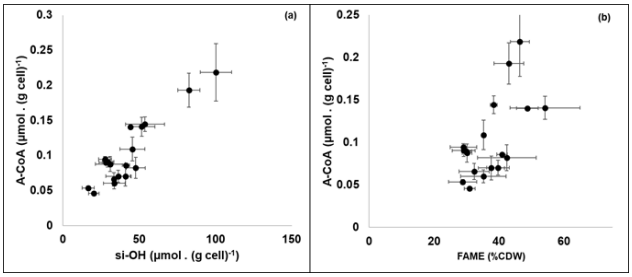

Figure 2: Relationship of aconitase with OS (a) and TAG (FAME) content (b). The specific aconitase activity correlated negatively with si-OH and FAME content.

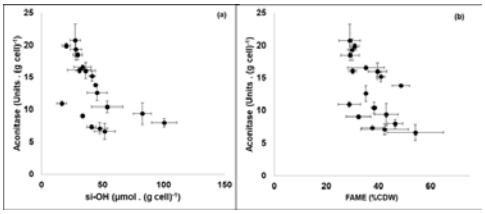

Figure 3: Relationship between aconitase activity and A-CoA levels. The specific aconitase activity poorly correlated with A-CoA levels.

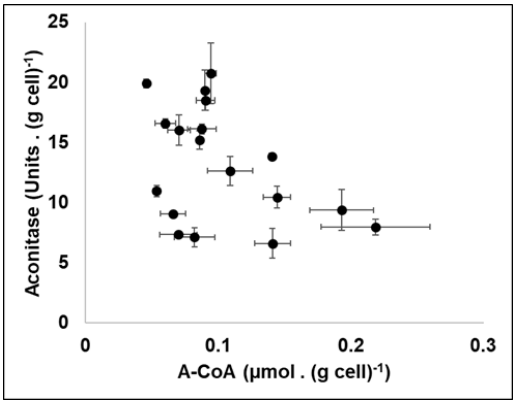

Figure 4: Pareto optimum chart-tradeoff between biomass and TAG storage. Improvement in TAG to various level is possible without trading off with biomass growth rate of 0.2 h^{-1}

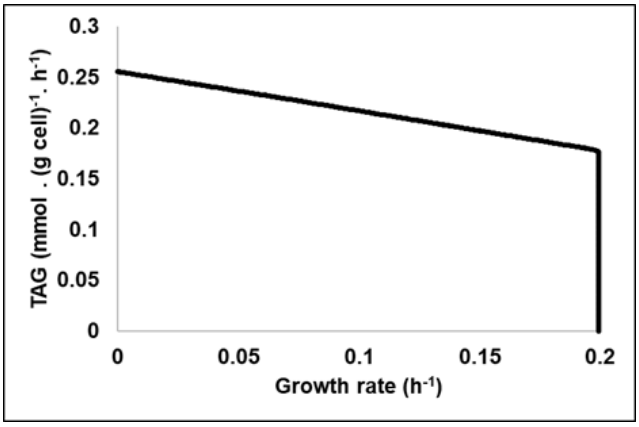

Figure 5: MOMA simulation: TAG storage flux and growth rate. Inactivation of triosephosphate isomerase (TPI) flux, but not aconitase (ACO) flux results in improved TAG storage flux when compared to control (a). With increasing flux constraint through TPI, a concomitant increase in G6PDH and TAG storage flux were observed (b).

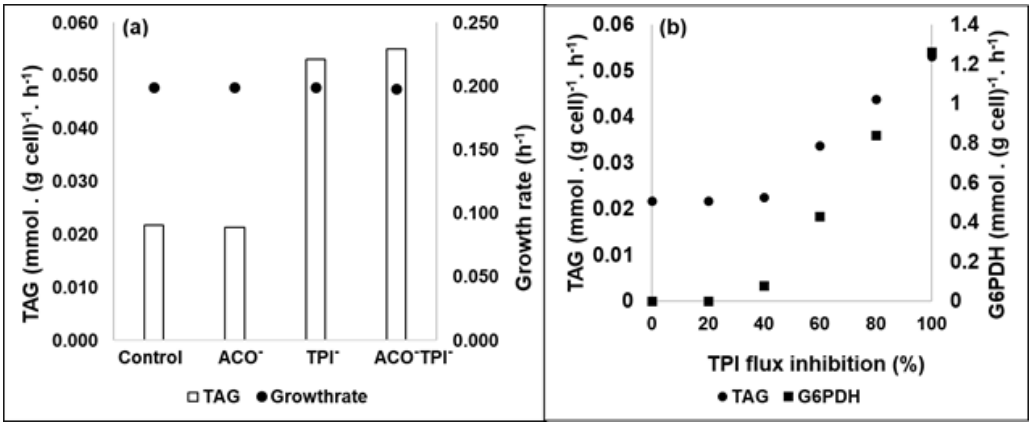

Figure 6: MOMA simulation: observed flux values of different reactions under unconstrained (control) and constrained aconitase (ACO^-) and TPI (TPI^-) fluxes. ACO-aconitase (a), TPI-triosephosphate isomerase (b), G6PDH-glucose-6-phosphate dehydrogenase (c), PK-phosphoketolase (d), PTA-phospho transacetylase (e), CL-citrate lyase (f), ACS-acetyl-CoA synthetase (g), AK-acetate kinase (h), ACCT- acetyl-CoA carboxylase carboxytransferase (i). In all the plots y-axis represents the respective flux in mmol $(g\ cell)^{-1}\ h^{-1}$. TPI^- had active flux through G6PDH and PK and improved PTA flux when compared to control and ACO^-. Both TPI^- and ACO^- improved the flux through ACCT

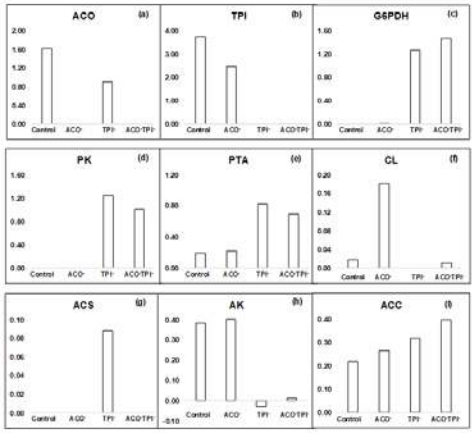

Figure 7: TPI and G6PDH activity of *R. opacus* PD630 at different time points. At 60% of the time points the TPI activity decreased and G6PDH activity increased under OS when compared to control.